Modeling of the Densification of Porous Molybdenum by a Unit Cell Approach

H.J. Böhm[1*], D. Duschlbauer[1], H.E. Pettermann[1], J. Segurado[2] and A. Plankensteiner[3]

[1]*Institute of Lightweight Structures and Aerospace Engineering, Vienna University of Technology, A–1040 Vienna, Austria*
[*] *Corresponding author: hjb@ilfb.tuwien.ac.at*

[2]*Department of Materials Science, Universidad Politécnica de Madrid, E–28040 Madrid, Spain*
[3]*Plansee AG, A–6600 Reutte, Austria*

ABSTRACT

Unit cell models are used to study the densification by compressive mechanical loading of molybdenum containing initially spherical pores at volume fractions between 2% and 10%. The model geometries correspond to body centered cubic arrangements of voids in a matrix. The stress and strain fields in the cells are solved for by the Finite Element Method. The molybdenum matrix is described by an elastoplastic material model and contact between the pore surfaces is provided for.

Densification up to very small residual porosities is modeled by the above continuum micromechanical approach for two levels of the overall stress triaxiality. The evolution of the shapes of the pores is found to be markedly influenced by the loading conditions and the pore geometries are predicted to differ markedly from ellipsoids at elevated degrees of densification.

1. INTRODUCTION

Due to the high melting points of refractory metals, products made of them are typically manufactured by powder metallurgy. Such production routes often involve hot working and heat treatment steps that are designed to remove the residual porosity remaining after sintering. The elimination of such pores, which tend to be homogeneously distributed in the matrix and show approximately spherical shapes, is of major importance in obtaining optimum material characteristics for components that are to be subjected to severe thermal and mechanical loads. Even though a considerable body of empirical knowledge exists with respect to the hot forming of porous refractory metals, experiments and modeling are required for obtaining a deeper understanding of such densification processes.

A considerable number of studies have been published on modeling the growth of pores in ductile media in the context of the ductile damage and failure of metals. Few reports, however, have aimed at simulating the densification of porous ductile materials. One group of them use numerical engineering methods to model

processing steps such as upsetting, the material behavior of the porous metal being obtained from constitutive descriptions based on micromechanical methods. Works involving a Gurson model /1/ and Hashin–Shtrikman estimates /2/ were published, the latter approach being capable of following the evolution of the shapes of ellipsoidal voids through the deformation process.

Another modeling strategy consists in carrying out detailed studies of the densification of porous metals at the microscale by unit cells. Segurado et al. /3/ reported a three-dimensional model of this type, the starting geometry of which is a body centered cubic array of spherical voids in a matrix, which are either of equal size or of two different sizes. Symmetry boundary conditions were prescribed and contact with rigid surfaces was used to avoid interpenetration of the void surfaces as the pores closed. An elastoplastic material description with hardening was employed for the metal, corresponding to the behavior of molybdenum at a temperature of 1000°C. This model was used for investigating the reduction of overall porosity and the evolution of pore shapes under conditions of uniaxial macroscopic compressive loading at different initial pore volume fractions. The evolved pore shapes were found to deviate significantly from ellipsoids, the predicted lens-like shapes being in qualitative agreement with experimental findings. This behavior differs markedly from the response of viscoplastic porous media under tensile loading, for which initially spherical pores were shown to remain ellipsoids throughout the deformation history for a wide range of macroscopic stress triaxialities /4/.

2. AXISYMMETRIC CELL MODELS

Three-dimensional unit cell models of the type used in /3/ are capable of handling many (but not all) load cases, among them sequential uniaxial loading in different directions, but are rather expensive computationally. For axisymmetric macroscopic stress states a more economic alternative consists in using axisymmetric models that approximate cubic arrays of voids by cylindrical cells (which are not unit cells in the strict sense). Tvergaard /5/ proposed boundary conditions for describing staggered arrays of particles or voids with such axisymmetric cells and his approach can be extended to handling particles or voids of different sizes /6/. In the latter scheme a pair of axisymmetric cells is considered, both of which are subjected to symmetry displacement B.C.s at their top and bottom surfaces, i.e., the axial displacement components v must fulfill the relations $v=0$ on B_1 and B_2, $v=v(M_1)$ on T_1 and $v=v(M_2)$ on T_2 with $v(M_1)=v(M_2)$ - compare Figure 1. On the outer surfaces of the cells, E_1 and E_2, pairs of "equivalent" points, P_1 and P_2, are constrained to have the same axial displacements, $v(P_1) = v(P_2)$. The radial displacements u of any such pair of points must be chosen such that the sum of the cross sectional areas of both cells is independent of the axial coordinate, leading to the condition

$$u^2(P_1) + u^2(P_2) = u^2(M_1) + u^2(M_2) \tag{1}$$

For most applications these nonlinear B.C.s can be linearized to give

$$u(P1) + u(P2) = u(M1) + u(M2) \tag{2}$$

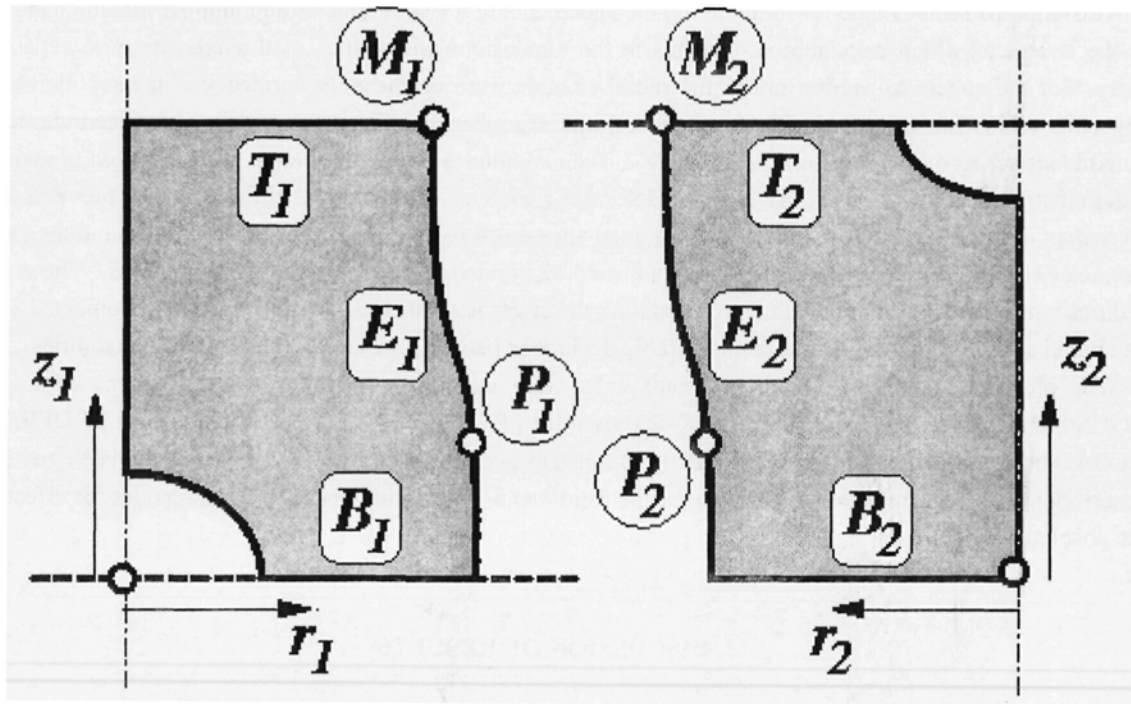

Fig. 1: Sketch of a pair of axisymmetric cells with pores of different size.

When low levels of residual porosity are to be attained, i.e. for pore volume fractions $\xi \to 0$, the closing of pores must be accounted for. For this purpose the interior surfaces of the voids were provided with contact surfaces that acted against rigid planes coupled to the faces B_1 and T_2, which are indicated by dotted lines in Figure 1.

For axisymmetric stress states there are two pairs of axial and radial stress components, $[\sigma_{zz}, \sigma_r]$, that lead to a given value of the stress triaxiality χ, which is defined as

$$\chi = \frac{\sigma_m}{\sigma_{eq}} = \frac{\frac{1}{3}(\sigma_{zz} + 2\sigma_r)}{|\sigma_{zz} - \sigma_r|} \tag{3}$$

Here σ_m stands for the mean (hydrostatic) stress and σ_{eq} is the von Mises equivalent stress. For the work discussed here, two levels of the macroscopic stress triaxiality were considered, $\chi = -\frac{1}{3}$, which can be obtained by applied stresses with axial and radial components $[\sigma_{zz}, \sigma_r]$ of $\sigma_0[-1, 0]$ and $\sigma_0/3[1, -2]$, as well as $\chi = -\frac{4}{3}$, for which the pairs of stress components are $\sigma_0/\sqrt{6}[-2, -1]$ and $\sigma_0/(3\sqrt{6})$ $[-2, -5]$. Obviously all of the above load cases give rise to compressive mean stresses for positive values of σ_0. For both triaxialities considered, the first pair of axial and radial stresses is dominated by axial compression and gives rise to increasingly oblate voids during the densification process ("sphere-to-crack" deformation modes), whereas the second pair is dominated by radial compression and leads to increasingly prolate voids ("sphere-to-needle" deformation modes).

Provision had to be made for maintaining the specified stress triaxialities throughout the loading histories, in the course of which considerable changes in the dimensions and shapes of the axisymmetric cells take place. For the sphere-to-needle modes the radial stresses were accordingly applied via linearly increasing concentrated loads acting on the master nodes M_1 and M_2, whereas axial stresses were introduced via distributed loads acting on the top surfaces T_1 and T_2. The magnitudes of the latter loads were adjusted to give the required stress triaxiality on the basis of the deformed geometry of the cell resulting from the previous load increment. For the sphere-to-crack modes the axial stresses were applied via the master nodes and the radial stresses (where necessary) via appropriately adjusted distributed loads acting on faces E_1 and E_2. These procedures amount to explicit algorithms for updating the stress triaxiality. Accordingly, load increments had to be chosen sufficiently small to avoid undesirable deviations between the actual and nominal triaxialities.

The stress and strain fields in the unit cells were evaluated with the Finite Element code ABAQUS/Standard V 5.8 (Hibbitt, Karlsson & Sorensen Inc., Pawtucket, RI), the user subroutines URDFIL and DLOAD being used to implement the loading at constant overall stress triaxialities. An elastoplastic material description with hardening was employed for the solid metal, so that the models cannot account for effects of the absolute size of voids.

3. DISCUSSION OF RESULTS

The axisymmetric cells were used to study the densification of porous molybdenum for three levels of initial porosity, ξ_0=0.10, ξ_0=0.06, and ξ_0=0.02, for each of which the sphere-to-crack and sphere-to-needle void deformation modes were evaluated for stress triaxialities of $\chi=-\frac{1}{3}$ and $\chi=-\frac{4}{3}$. In addition, starting configurations with voids of equal size (volume ratio q=1.0) and with two types of differently sized voids (volume ratio q=4.1) were considered; for details see /7/. Loading conditions of all the above types can be encountered at different positions in work pieces undergoing processing for the removal of residual porosity.

Excellent agreement with three-dimensional unit cell models was found in terms of both the overall strain vs. density diagrams and of the evolution of the shapes of the voids in the sphere-to-crack deformation mode at $\chi=-\frac{1}{3}$. This indicates that the linearized radial B.C.s for the axisymmetric cells, eqn.(2), did not degrade the results despite the considerable deformations involved in the problems. Figure 2 shows the predicted contours of the microscopic equivalent plastic strains in the solid molybdenum and the deformed shapes of such a pair of axisymmetric cells at two levels of the overall equivalent strain, which was evaluated as, $\varepsilon_{eq} = 2/3\,|\,\varepsilon_{zz} - \varepsilon_r\,|$. The smaller voids (right) can be seen to close at lower overall strains than the bigger ones (left). The lens-like shapes of the voids in highly deformed states are evident. Regions of high plastic strains are associated with the ring-shaped zones of extreme curvature at the equators of the pores.

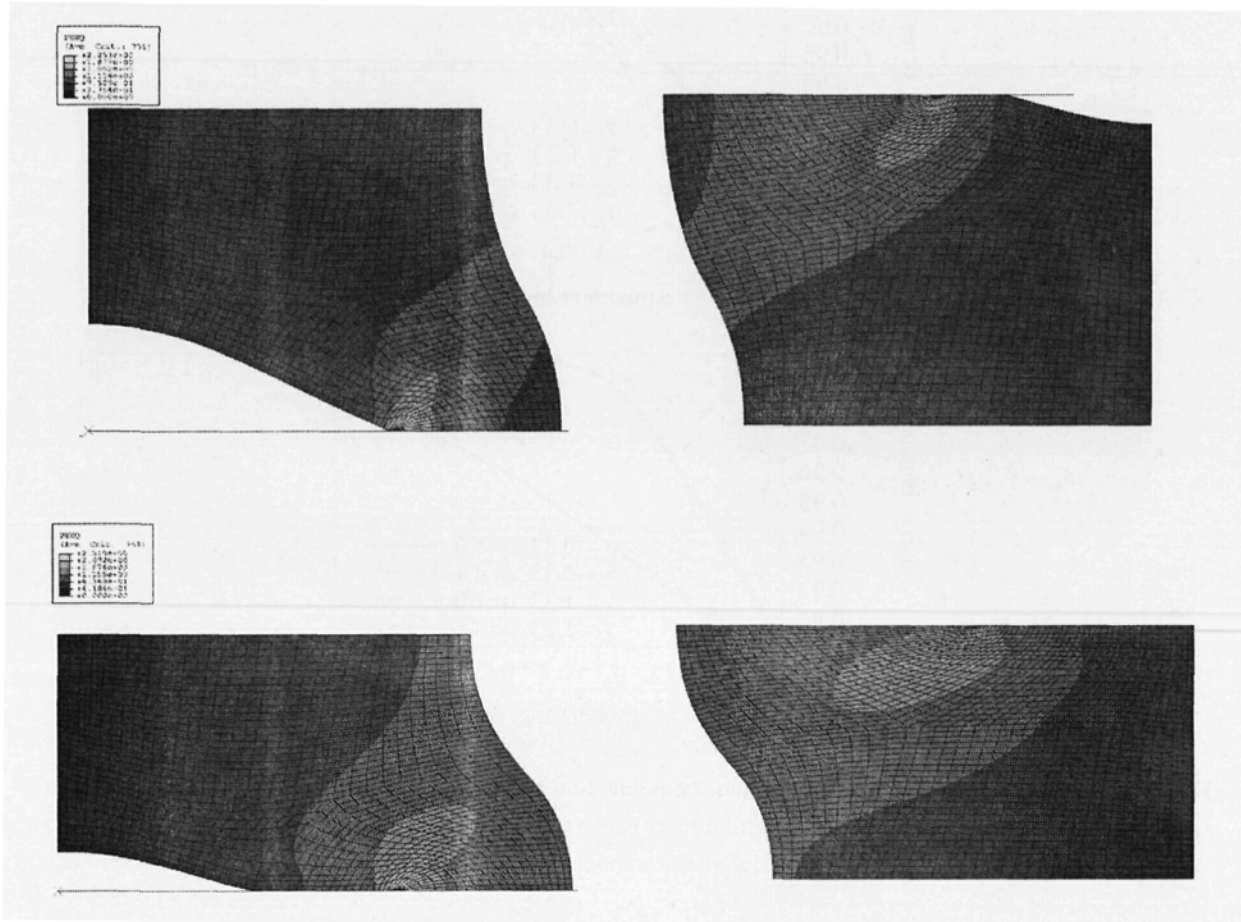

Fig. 2: Contour plots of the distributions of the equivalent plastic strains in the solid metal at overall equivalent strains of ε_{eq}=0.346 (upper row) and ε_{eq}=0.581 (lower row) predicted for a macroscopic stress triaxiality $\chi=-\frac{1}{3}$ (sphere-to-crack deformation mode) and initially spherical pores of two different sizes (initial volume ratio q=4.1, initial total void volume fraction ξ_0=0.10).

Predictions for the evolution of the relative density of the porous metal as function of the overall equivalent strain are presented in Figure 3 for an initial void volume fraction of ξ_0=0.10 (initial relative density ρ_0=0.90). Results corresponding to the sphere-to-crack (left) and sphere-to-needle (right) deformation modes are shown for stress triaxialities of $\chi=-\frac{1}{3}$ and $\chi=-\frac{4}{3}$ and for void volume ratios of q=1.0 (equally sized voids) as well as q=4.1 (two populations of voids).

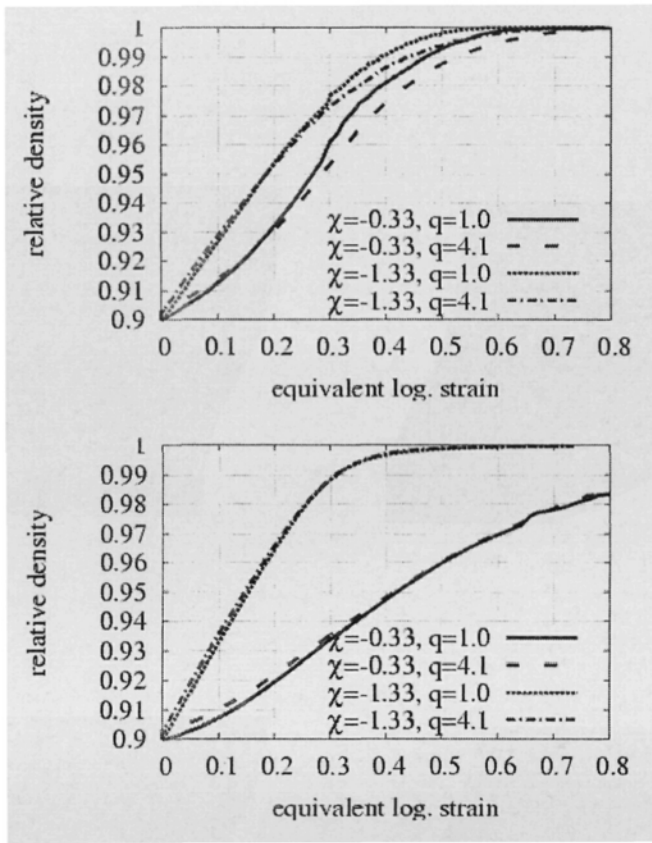

Fig. 3: Predicted evolution of the relative density as function of the overall equivalent strain during the compaction of porous molybdenum (initial total void volume fraction ξ_0=0.10) for sphere-to-crack (left) and sphere-to-needle (right) pore deformation modes.

The deformation mode of the voids and the overall stress triaxility can be seen to exert a dominating influence on the densification behavior, with χ playing an especially important role in the sphere-to-needle case. Essentially full densification was achieved for the sphere-to-crack mode at both stress triaxilities considered and for the sphere-to-needle mode at $\chi=-\frac{4}{3}$. In contrast, the relative density remained below ρ=0.985 for the sphere-to-needle deformation mode at a stress triaxiality of $\chi=-\frac{1}{3}$ throughout the loading sequence considered. The effects of the relative pore sizes on the overall response, while evident in Figure 3, were found to be rather more limited. An evaluation of the results in terms of the total strain energy density /7/ indicates, on the one hand, a pronounced increase of the strain energy per unit cell in the final stages of densification and, on the other hand, a tendency for the sphere-to-needle deformation modes to require more energy for full densification than the sphere-to-crack modes. The latter effect is especially marked for a stress triaxiliality of $\chi=-\frac{1}{3}$, the behavior of which can be partially explained by noting that this load case specifies tensile deformation in axial direction.

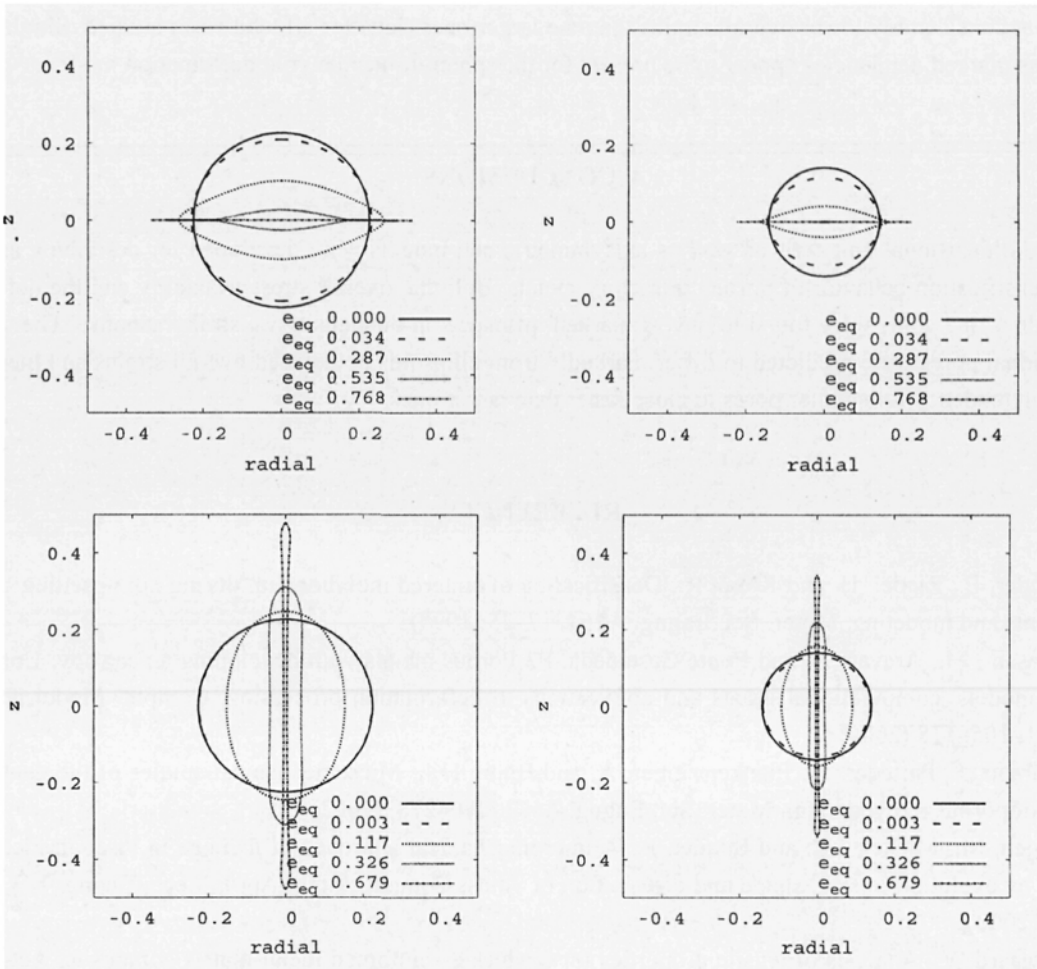

Fig. 4: Evolution of the shapes of initially spherical large (left) and small (right) pores of volume ratio q=4.1 and initial total void volume fraction ξ_0=0.06 predicted for a macroscopic stress triaxiality $\chi = -\frac{4}{3}$. Results for the sphere-to-crack (top) and sphere-to-needle (bottom) void deformation modes are shown.

Figure 4 displays the evolution of the pore shapes for two populations of initially spherical voids, the initial void volume fraction being ξ_0=0.06 and the initial volume ratio q=4.1. Predictions for the sphere-to-crack deformation mode are shown in the top row and those for the sphere-to-needle mode in the bottom row, the overall stress triaxiality being $\chi = -\frac{4}{3}$ in both cases. The void shapes are approximately ellipsoidal for overall equivalent strains up to, say, ε_{eq}=0.2, but differ markedly from ellipsoids at elevated overall strains despite the relatively high triaxiality considered. In the sphere-to-crack deformation mode shows the pore surfaces achieved contact in all cases considered. This leads to bonding at the high temperatures present during the solidification process and has a marked influence on the resulting pore shapes. The sphere-to-needle mode, in contrast, tends to give rise to elongated pores of low volume fraction, in which there is no contact between the surfaces. For the sphere-to-crack deformation mode the smaller voids (right) were found

to close at considerably lower overall strains than the larger ones (left) for all load cases studied. Similar, but much less marked, tendencies appear to be present for the sphere-to-needle void deformation mode.

4. CONCLUSIONS

Three-dimensional unit cells as well as axisymmetric cell models were developed for describing aspects of the densification behavior of porous refractory metals. Both the overall stress triaxiality and the deformation mode of the voids were found to have a marked influence on the density vs. strain response. The shapes of individual pores were predicted to differ markedly from ellipsoids at elevated overall strains and there is a consistent tendency for smaller pores to close faster than larger ones.

REFERENCES

1. Parteder, E., Riedel, H. and Kopp, R., Densification of sintered molybdenum during hot upsetting: Experiments and modeling, Mater. Sci. Engng. A264, 17–25 (1999).
2. Kailasam, M., Aravas, N. and Ponte Castañeda, P., Porous metals with developing anisotropy: Constitutive models, computational issues and applications to deformation processing, Comput. Model. Engng. Sci. 1, 105–118 (2000).
3. Segurado, J., Parteder, E., Plankensteiner, A. and Böhm H.J., Micromechanical studies of the densification of porous molybdenum, Mater. Sci. Engng. A333, 270–278, (2002).
4. Gărăjeu, M., Michel, J.C. and Suquet, P., A micromechanical approach of damage in viscoplastic materials by evolution in size, shape and distribution of voids, Comput. Meth. Appl. Mech. Engng. 183, 223–246 (2000).
5. Tvergaard, V., Analysis of tensile properties for a whisker-reinforced metal-matrix composite, Acta metal. mater. 38, 185–194 (1990).
6. Weissenbek, E., Böhm, H.J. and Rammerstorfer, F.G., Micromechanical investigations of arrangement effects in particle reinforced metal matrix composites, Comput. Mater. Sci. 3, 263–278 (1994).
7. Plankensteiner A.F., Duschlbauer D., Coube O., Pettermann H.E. and Riedel H., Numerical and experimental analysis of pore shape evolution of sintered Molybdenum under triaxial Loading conditions, to be published in Proc. 2003 International Conference on Powder Metallurgy and Particulate Materials (PM2TEC), Las Vegas, NV, June 2003.